ISSN 1392-1207. MECHANIKA. Vol. 30, No. 5, 2024: 408−414

Elasticity Study of SLA Additively Manufactured Composites

Alireza SHAHIDI*, Karolis STRAVINSKAS*, Ada STEPONAVIČIŪTĖ*, Artūras KILIKEVIČIUS, Darius VAINORIUS**, Jonas MATIJOŠIUS**, Oleksandr KAPUSTYNSKYI**, Genrik MORDAS***

**Center for Physical Sciences and Technology, LT-02300 Vilnius, Lithuania,*
E-mails: alireza.shahidi@ftmc.lt, karolis.stravinskas@ftmc.lt, ada.steponaviciute@ftmc.lt, genrik.mordas@ftmc.lt
***Faculty of Mechanics, Vilnius Gediminas Technical University, Saulėtekio al. 11, 10221 Vilnius, Lithuania,*
E-mails: arturas.kilikevicius@vilniustech.lt, darius.vainorius@vilniustech.lt, jonas.matijošius@vilniustech.lt, o.kapustynskyi@vilniustech.lt

https://doi.org/10.5755/j02.mech.37478

1. Introduction

Ceramics have long been revered for their exceptional properties, including remarkable strength [1], superior thermal resistance [2], and excellent wear resistance [3]. These characteristics have propelled them to become vital materials in diverse industries. However, traditional manufacturing techniques often limit the creation of intricate geometries [4] and hinder the tailoring of functionalities [5], restricting their application in advanced fields.

The emergence of additive manufacturing (AM), also known as 3D printing, has revolutionized the manufacturing landscape. This groundbreaking technology offers unprecedented design freedom [6, 7], allowing the fabrication of complex structures that were previously unimaginable. Within the realm of AM, stereolithography (SLA), a technique that uses a photopolymer resin, emerges as a promising approach for the creation of ceramic composites [8]. Photopolymers are light-sensitive resins that solidify upon exposure to a specific light source [6], paving the way for the layer-by-layer construction of the desired shapes.

The SLA process employs a UV laser to selectively cure the photopolymer, meticulously building the object from a digital model [7]. This opens the door to the fabrication of intricate geometries that defy the limitations of conventional methods. Furthermore, by strategically incorporating ceramic fillers into the photopolymer, SLA facilitates the creation of functional ceramic composites with enhanced strength, improved thermal or electrical properties, and customized functionalities, catering to the demands of numerous sectors [9, 10].

These composites present exciting possibilities for applications requiring both intricate geometries and superior performance, such as aerospace components [4], lightweight yet robust heat exchangers [11], and biocompatible implants for medical applications [5].

Recent research has made significant strides in advancing the field of SLA-based ceramic composite fabrication. For example, Zhang et al. (2023) successfully demonstrated 3D printing of alumina-based composites with superior mechanical properties compared to traditional techniques [4]. Similarly, Li et al. (2022) explored the development of biocompatible composites for bone tissue engineering using SLA [5].

Stereolithography (SLA) 3D printing has established itself as a valuable tool for creating complex and highly precise prototypes and end-use parts [14]. However, conventional photopolymer resins lack the mechanical properties that are often required for functional applications. This has led to the exploration of ceramic and photopolymer composites, which offer a promising avenue to bridge this gap.

Photopolymerization, the core principle behind SLA, involves the use of light to initiate the formation of polymer chains from liquid monomers [15]. This process is typically based on photoinitiators that react to light, generating free radicals that subsequently trigger chain growth and solidification of the resin [16]. Ceramic particles are incorporated into these photopolymers to enhance their mechanical properties, including strength, stiffness, and wear resistance [17]. However, achieving a uniform dispersion of ceramic particles and ensuring their compatibility with the photopolymer matrix present significant challenges [18].

Recent studies have explored various approaches to overcome these challenges. One technique involves using silane coupling agents to modify the surface of ceramic particles, improving their compatibility with the polymer matrix, and promoting better dispersion [19]. Furthermore, researchers have investigated novel photopolymer formulations with tailored properties, such as high viscosity, to accommodate the higher ceramic content [20]. Furthermore, advanced printing parameters and post-processing techniques are being explored to optimize the printing process and achieve desired mechanical properties in the final parts [21, 22].

While still in development, ceramic and photopolymer composites hold immense potential to expand the capabilities of SLA 3D printing in various application domains. Continuous research efforts are focused on optimizing material formulations, printing processes, and post-processing techniques to achieve high-performance ceramic parts with customized properties.

The elastic behavior of materials is crucial for predicting deformations, as it allows for the estimation of how a material will change under load and whether it will return to its original state after the load is removed. This property also helps in determining strength limits and preventing failure. Understanding elasticity enables the optimization of material selection for various applications, ensuring its efficiency and durability. The elastic behavior of linearly elastic isotropic solids is characterized by two main constants: Young's modulus (E) and the shear modulus (G). These constants are crucial for the engineering design of structures. Consequently, many experimental methods have been devised to determine the values of E and G, which can be

broadly categorized into static and dynamic methods. The longitudinal dynamic modulus of elasticity is a key mechanical property of timber rectangular beams and can be measured using various vibration techniques, such as free or forced, flexural or longitudinal vibrations, under different support conditions.

The aim of the paper is to investigate the mechanical properties of ceramic and photopolymer composites created using stereolithography (SLA) 3D printing, specifically focusing on the dynamic testing methods for determining Young's modulus. The research seeks to evaluate and compare the performance of two SLA 3D printing materials, Liqcreate Composite-X and Phrozen's Water-Washable Resin, by employing dynamic flexural vibration tests to assess their natural frequencies and calculate their respective Young's moduli. Because material manufacturers do not provide such valuable information, it becomes challenging to use the materials effectively for subsequent engineering purposes. The ultimate goal is to advance the understanding and application of SLA-based ceramic composites in various high-performance engineering domains.

2. Object of the Study

Two of the most popular SLA 3D printing materials Liqcreate Composite-X and Phrozen Water-Washable Resin were used (Table 1 and Table 2).

Liqcreate Composite-X is a photopolymer resin for SLA 3D printing with excellent mechanical properties [12]. It contains pentaerythritol tetraacrylate for UV-induced crosslinking and solidification, with esterification products that improve printability and mechanics]. Diphenyl (2,4,6-trimethylbenzoyl) phosphine oxide serves as the photoinitiator for polymerization [3]. The resin's optimal printing uses a UV light source within 385-420 nm, and its mechanical properties are enhanced by post-curing under UV light or thermal treatment at 60°C for one hour or 100°C for two hours [12].

Phrozen's Water-Washable 3D Printing Resin is an environmentally friendly photopolymer designed for simple and safe post-processing, eliminating the need for toxic solvents [13]. Made with a urethane acrylate oligomer and reactive diluents, it offers good mechanical properties and fast curing speeds, thanks to photoinitiators. This resin is easily washable in water, facilitating the cleaning of 3D-printed objects. It requires specific UV light exposure for printing and post-curing to ensure the mechanical stability [13].

Table 1

Properties of Liqcreate Composite-X [12]

Property	Value
Tensile strength	50-75 MPa
Flexural strength	140-150 MPa
Hardness	93-94 Shore D
Viscosity	1400 cPs at 25°C
Glass transition	>100°C

Table 2

Properties of Phrozen water-washable resin [13]

Property	Value
Tensile strength	50 -60 MPa
Flexural strength	-
Hardness	75-85 Shore D
Viscosity	600-800 cPs
Glass transition	>87°C

3. Methodology for 3D SLA Printing

The 3D model for SLA printing created using the Fusion 360 student version software package (Fig. 1). For samples production, the Phrozen Sonic Mini Resin 3D Printer device was utilized (Table 3).

Used slicer software Chitubox (Resin 3D Printing Slicer) BasicV2 (version Basis V2.2.0) with parameters mentioned in Table 4.

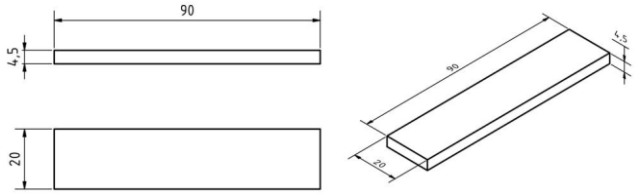

a

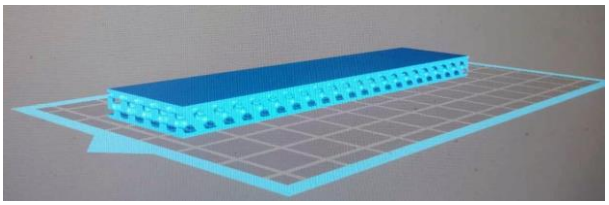

b

Fig. 1 View of the sample: a – the principal view, b –3D model (2.5D X-cell lattice structure, volume 40%)

Table 3

Phrozen sonic mini resin 3D printer technical data [34]

Technology	Resin 3D Printer
Type	LCD
Light Source	405nm ParaLED Matrix 2.0
XY Resolution	62.5 µm
Layer Thickness	0.01-0.30 mm
Maximum Printing Speed	80 mm/ hour

Table 4

Slicing parameters

Layer height	0.05 mm
Retract speed	150 mm/min
Lift distance	6 mm
Lift speed	60 mm/min

For both samples, the exposure time was set to 8 seconds and the rest delay time to 2 seconds. Given the high viscosity of composite X material and its inability to flow due to its weight, as well as the inadequate coverage on the platform, the rest delay time was initially increased. Subsequently, a mechanical mechanism was implemented to move the material laterally, ensuring that the area beneath the platform was fully covered with the material. This approach solved the issue of sample adhesion. Consequently, a uniform and reproducible sample structure was produced.

Printing parameters:

- Liqcreate Composite-X - first layer time 160 s, other layers 6 s. Interlayer delay time set to 8 seconds for material movement and filling of the whole surface.

- Phrozen Water-Washable Resin - first layer 40 s other layers 2 s. Interlayer delay time set by 4 seconds for material movement and filling of the whole surface.
- Post-curing time - >60 minutes at 60°C

4. Methodology for Sample Analysis

Material characterization plays a crucial role in various engineering applications. Traditionally, static and dynamic testing methods have been used to assess the mechanical properties of materials [23]. Among these properties, Young's modulus, yield strength, and tensile strength are of paramount importance, as they govern the response of a material to load [24].

Although static testing has been the established technique for determining Young's modulus, advances have facilitated the adoption of dynamic testing methods such as ultrasound and resonant vibration [25]. These dynamic approaches offer several advantages. They utilize small deformations, well below the elastic limit of the material, making the tests completely non-destructive [26]. This allows repeated testing of the same sample, which can be highly beneficial for generating statistically robust data [27].

From the perspective of conducting the experiments, the method involves two stages: initially, excitation and signal acquisition and processing are carried out to identify the natural frequencies; subsequently, mathematical relationships and computational methods are applied to derive (E) from these natural frequencies. Essentially, there are three types of vibration modes that can be employed to determine Young's modulus of a prismatic beam with an asymmetric cross-section around one axis, specifically out-of-plane and in-plane bending modes, as well as the longitudinal vibration mode. Research by other scientists indicates that sweep-sine excitation or short-duration excitation within a controlled frequency range yields better results [20]. Generally, when using bending vibration modes, a slender beam adhering to the Euler-Bernoulli theory is selected as the test specimen. For this purpose, the length (L) to thickness (h) ratio must exceed 20 [7]. By knowing the end conditions, we can establish the mathematical relationship between Young's modulus (E) and the beam dimensions (L, B, H), weight (m), and natural frequencies (f_i).

$$E = \frac{mL^3}{I}\left(\frac{2\pi f_i}{\alpha_i^2}\right)^2, \tag{1}$$

where I represents the moment of inertia of the cross-sectional area, calculated as $I = BH^3/12$, and α_i are coefficients that depend on the beam's support conditions and the mode numbers.

Table 5 displays the first two coefficients determined for a beam with fixed-free end conditions, commonly known as a cantilever beam.

For the determination of Young's modulus using flexural vibration tests, specific procedures are followed [28].

The length of the beam used in the dynamic test was 90 mm, thickness 4.5 mm, width 20 mm. The main indicator of the geometry selection was the L/H ratio, which was chosen to be 20 as recommended by the review of scientific articles [28]. The average mass density of the objects under investigation was experimentally determined by dividing their mass by volume [24]. An electronic analytical balance, Kern ABP-200-4M, with a weighing capacity of up to 13.38 g for "Liqcreate Composite-X" materials and 9.5 g for "Phrozen's Water-Washable" materials, and a resolution of 0.1 mg, was used for these density measurements [24]. Due to limitations in the available equipment, the value of theoretical mass density was ultimately used in the calculations of Young's modulus.

Table 5

Dimensionless coefficients α_n used to compute the frequencies of a cantilever beam.

Mode number	1	2
α_n	1.8751	4.6941

The bending vibration test was performed on a dedicated test table designed to isolate the system from external noise and vibrations [29]. The "Brüel & Kjær" vibration measurement equipment comprised the following components:

1. Portable data acquisition system (3660-D) for processing, storing, and managing measurement results.
2. A personal computer (DELL).
3. Non-contact inductive position measurement sensors (U20B and U3B) from "Lion precision" with amplifiers and an opacity source.
4. Excitation vibrator (4810) with an amplifier and a frequency generator.

Each specimen was prepared for vibration detection by adhering a very thin aluminium foil to 15 designated points. The test specimens were then securely clamped at one end. The displacement of each point was measured using the small displacement sensor (U3B). A larger sensor (U20B) was placed on a heavy metal base to detect stable ground level and any vibrations of the entire system, including the test table [29].

Dynamic tests were performed (frequency sweep excitation) [30]. In the frequency sweep method, the specimen was stimulated across a range of frequencies (100 Hz to 1000 Hz) at a sweep rate of 500 Hz/s to induce various vibrational modes [30]. During excitation at each point, the swept sine signal was repeated multiple times, and the frequency response was monitored. The impact method involved striking the free end of the specimen with a hammer to avoid resonance in the system and sensors, thereby obtaining accurate natural frequency values. Following impact, the specimen vibrated freely in its vertical modes, and all vibrations exhibiting a gradual decrease in amplitude over time. Although this impact method can be useful for predicting the initial few resonant modes, it is less effective for investigating higher frequencies [30]. As highlighted in various research studies [31], the most accurate Young's modulus calculations are derived from the first resonant modes. Consequently, focusing on higher-frequency modes would offer minimal benefit [31].

In both experiments, the signals from both sensors were processed by portable equipment (3660-D) and transmitted to the PC, where the displacement of each point was plotted for analysis.

Two beams with identical dimensions but different materials ("Liqcreate Composite-X" and "Phrozen's Water-Washable") were chosen for the cantilever beam tests [32].

Fig. 2, a shows the model and geometric characteristics of the cantilever beam with a square cross section used in the experimental modal analysis [32]. The measurement system, sensor location, and beam fixation method are illustrated in Fig. 2, b [33]. Brüel&Kjær PULSE software was employed to conduct the experiments [33].

In performing the experimental modal analysis, operational modal analysis (OMA) was used, the structure of which is presented in Fig. 2, c.

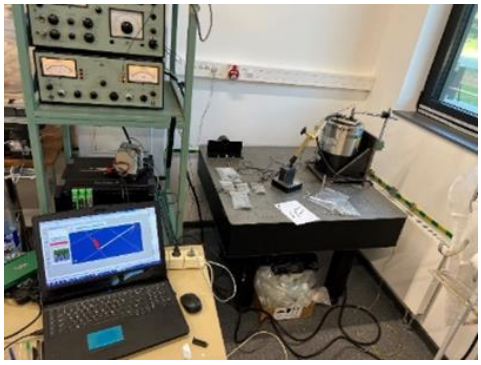

a

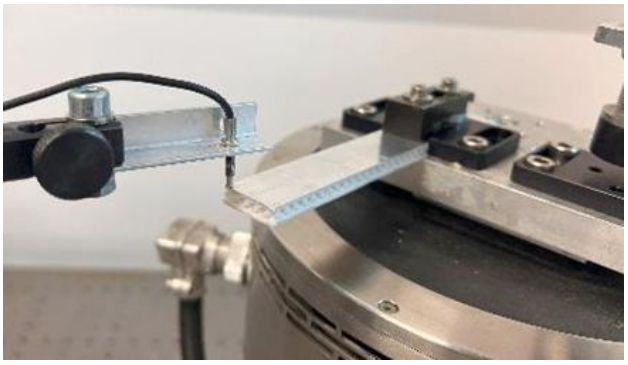

b

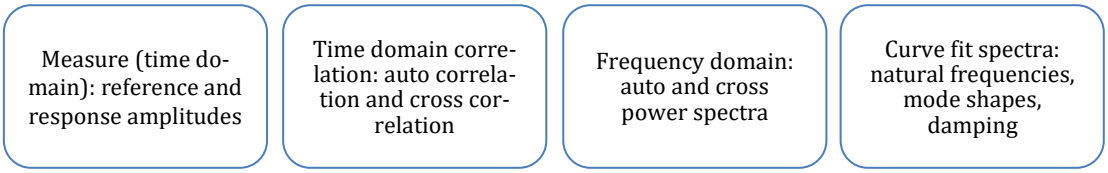

c

Fig. 2 General view of the testing stand (a), view of the specimen fixation (b), and operational modal analysis (c)

5. Results

The research objects are the 3D printed, Liqcreate Composite-X" "Phrozen Water-Washable" and which are presented in Fig. 3. The set of 12 specimens (6 for each materials) was 3D printed and prepared for vibration detection by adhering very thin aluminium foil to 15 designated points (aluminium foil with a thickness of 100 microns was stuck to the sample during harmonic analysis on the opposite side of the hall effect sensor).

Vibrational measurements in the vertical direction were conducted at 15 points on the corresponding specimen (Fig. 3). The response results from one of the measurement points on the specimens are presented in Fig. 4.

The results of the OMA are presented in Table 6 and 7. The first two resonance frequencies with clearly defined modes, whose shapes are shown in Fig. 5, were determined using OMA. The automatically detected resonant frequency of the first and second bending modes of the samples was used for calculation of Young's modulus. The Young's modulus of the Phrozen Water-Washable Resin established by the resonant frequency method exceeds only $(3 \pm 0.3)10^{10}$ Pa and for Liqcreate Composite-X it exceeds $(6 \pm 0.93)10^{10}$ Pa (Table 6). The values of Young's modulus for each material are determined according to Eq. (1).

Fig. 3 Liqcreate Composite-X (left, white) and "Phrozen's Water-Washable (right, grey) samples

Table 6

Different mode shape natural frequencies of composite and resin samples

Mode No.	Frequency [Hz]	
	Liqcreate Composite-X	Phrozen Water-Washable resin
Mode 1	318 ± 10	210 ± 8
Mode 2	479 ± 13	578 ± 15

Table 7

Experimental natural frequencies and Young's modulus of composite and resin samples

Sample	Frequency of first resonant mode	Young's modulus determined after dynamic test (frequency of first bending mode), Pa
Liqcreate Composite-X	318 ± 10	$(6 \pm 0.93)10^{10}$
Phrozen Water-Washable Resin	210 ± 8	$(3 \pm 0.3)10^{10}$

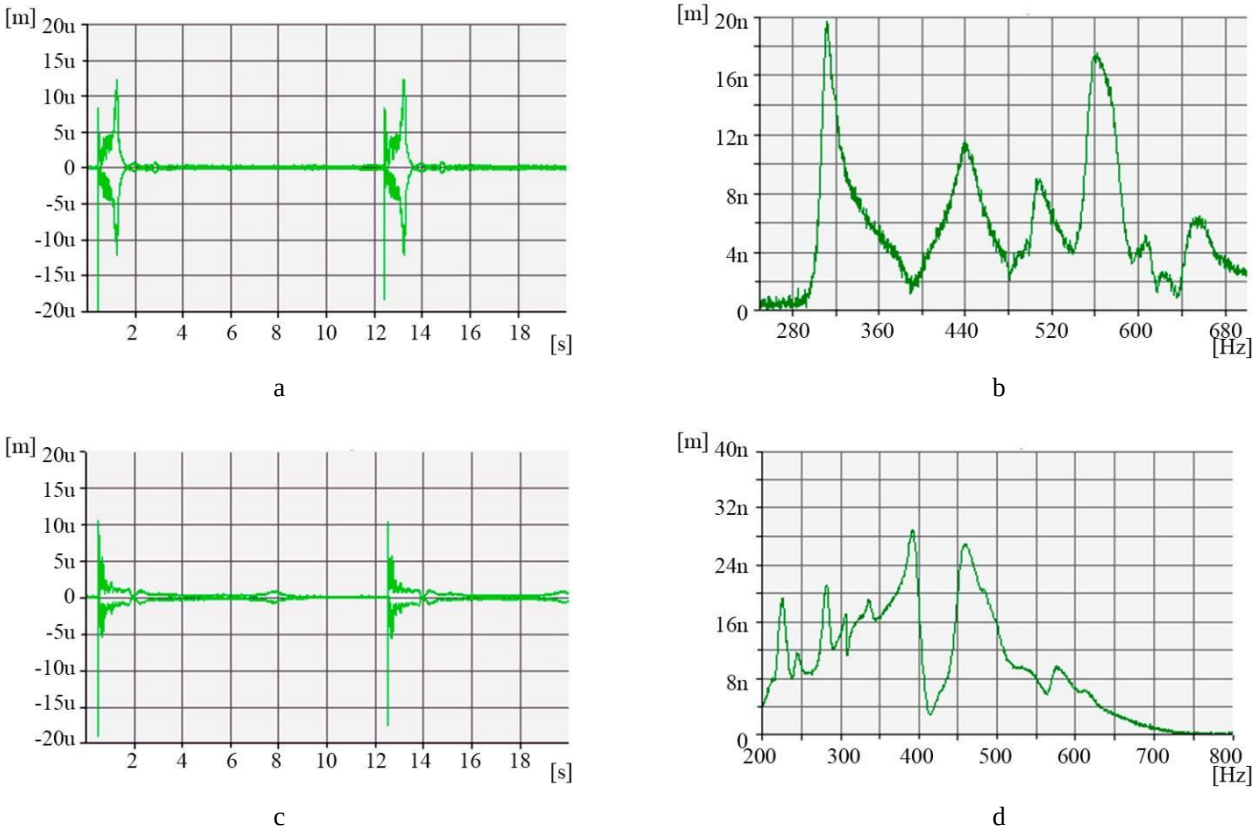

Fig. 4 Time histories and frequency spectra of displacement amplitudes of the sample point: a, b – Liqcreate Composite-X, c, d – Phrozen's Water-Washable

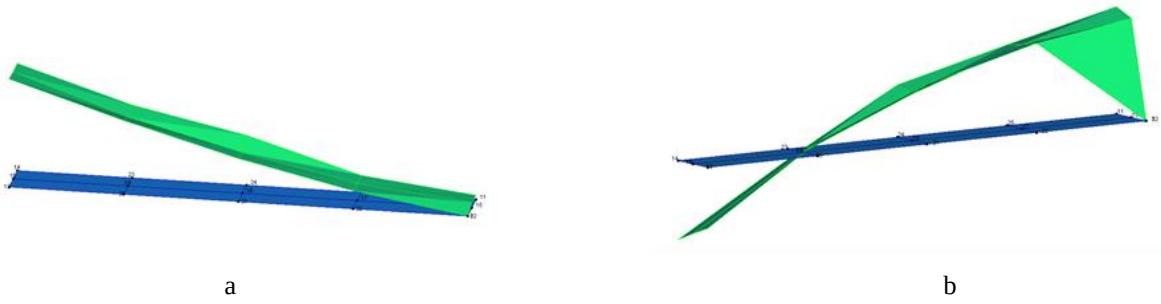

Fig. 5 Results of OMA of the sample: a – shape of first resonant mode of sample; b – shape of secondary resonant mode of sample

6. Conclusions

The study found that "Liqcreate Composite-X" had a first resonance frequency of 318 Hz, while "Water-Washable Resin" had a first resonance frequency of 210 Hz. Consequently, the Young's modulus of "Liqcreate Composite-X" was 0.93 x 10^{10} Pa, significantly higher than the 0.30 x 10^{10} Pa of "Water-Washable Resin."

"Liqcreate Composite-X" demonstrates superior mechanical performance with higher natural frequencies and a greater Young's modulus, making it suitable for applications requiring high strength and stiffness. "Phrozen's Water-Washable Resin," while easier to process and environmentally friendly, has lower mechanical properties, making it more suitable for less demanding applications.

This study underscores the importance of material selection in SLA 3D printing for applications with specific mechanical requirements.

In addition, this study confirms that the data officially presented by the manufacturers of these products and similar products in general is not sufficient to form data on future products that will be printed on a 3D printer and especially their mechanical properties. This makes it impossible to quickly select materials to print important structures without additional testing.

References

1. **Basutkar, A. G.; Kolekar, A.** 2015. A Review on Properties and Applications of Ceramic Matrix Composites, International Journal of Research and Scientific Innovation 2(12): 28-30. Available at: https://rsisinternational.org/Issue21/28-30.pdf.
2. **Belmonte, M.** 2006. Advanced Ceramic Materials for High Temperature Applications, Advanced Engineering Materials 8(8):693-703. http://dx.doi.org/10.1002/adem.200500269.
3. **Zhang, W.** 2021. A review of tribological properties for boron carbide ceramics, Progress in Materials Science 116: 100718.

https://doi.org/10.1016/j.pmatsci.2020.100718.
4. **Coppola, B.; Lacondemine, T.; Tardivat, C.; Montanaro, L.; Palmero, P.** 2023. Designing alumina-zirconia composites by DLP-based stereolithography: Microstructural tailoring and mechanical performances, Ceramics International 47(10), Part A: 13457-13468. https://doi.org/10.1016/j.ceramint.2021.01.204.
5. **MacDonald, A. F.; Harley-Troxell, M. E.; Newby, S., D.; Dhar M. S.** 2022. 3D-Printing Graphene Scaffolds for Bone Tissue Engineering, Pharmaceutics 14(9): 1834. https://doi.org/10.3390/pharmaceutics14091834.
6. **Goh, G. D.; Yap, Y. L.; Agarwala, S.; Yeong, W. Y.** 2019. Recent Progress in Additive Manufacturing of Fiber Reinforced Polymer Composite, Advanced Materials Technologies 4(1): 1800271. https://doi.org/10.1002/admt.201800271.
7. **Bártolo, P. J.** (Ed.). 2011. Stereolithography. New York: Springer. 340p. https://doi.org/10.1007/978-0-387-92904-0.
8. **Zamani, Y.; Amoabediny, G.; Mohammadi, J.; Seddiqi, H.; Helder, M. N.; Zandieh-Doulabi, B.; Klein-Nulend, J.; Koolstra, J. H.** 2020. 3D-printed poly(Ɛ-caprolactone) scaffold with gradient mechanical properties according to force distribution in the mandible for mandibular bone tissue engineering, Journal of the Mechanical Behavior of Biomedical Materials 104: 103638. https://doi.org/10.1016/j.jmbbm.2020.103638.
9. **Chen, Z.; Li, Z.; Li, J.; Liu, C.; Lao, C.; Fu, Y.; Liu, C.; Li, Y.; Wang, P.; He, Y.** 2019. 3D printing of ceramics: A review, Journal of the European Ceramic Society 39(4): 661-687. https://doi.org/10.1016/j.jeurceramsoc.2018.11.013.
10. **Wang, S.; Xiang, Y.; Feng, H.; Cui, Y.; Liu, X.; Chang, X.; Guo, J.; Tu, P.** 2024. Optimization of 3D Printing Parameters for Alumina Ceramic Based on the Orthogonal Test, ACS Omega 9(14): 16734–16742. https://doi.org/10.1021/acsomega.4c00819.
11. **Zou, Y.; Li, C-H.; Hu, L.; Liang, X.; Zhou, N-Y.; Li, Y-W.; Shi, Y-S.** 2024. Comparative study of SiC fabrication through 3D-printing combining silicon infiltration based on granulated and non-granulated powders, Ceramics International (in press, corrected proof). https://doi.org/10.1016/j.ceramint.2024.09.363.
12. Liqcreate Composite-X. Available at: https://www.liqcreate.com/product/composite-x/.
13. Phrozen Water-Washable 3D Printer Resin. Available at: https://makersuite.net/products/phrozen-water-washable-3d-printer-resin.
14. **Lim, D.-S.; Chung, J.-K.; Yun, J.-S.; Park, M.-S.** 2023. Fabrication of 3D Printed Ceramic Part Using Photo-Polymerization Process, Polymers 15(7): 1601. https://doi.org/10.3390/polym15071601.
15. **Chiulan, I.; Heggset, E. B.; Voicu, S. I.; Chinga-Carrasco, G.** 2021. Photopolymerization of Bio-Based Polymers in a Biomedical Engineering Perspective, Biomacromolecules 22(5): 1795–1814. https://doi.org/10.1021/acs.biomac.0c01745.
16. **Peng, B.; Yang, Y.; Gu, K.; Amis, E. J.; Cavicchi**, **K. A.** 2019. Digital Light Processing 3D Printing of Triple Shape Memory Polymer for Sequential Shape Shifting, ACS Materials Letters 1(4): 410–417. https://doi.org/10.1021/acsmaterialslett.9b00262.
17. **Abdelkader, M.; Petrik, S. Nestler, D.; Fijalkowski M.** 2024. Ceramics 3D Printing: A Comprehensive Overview and Applications, with Brief Insights into Industry and Market, Ceramics 7(1):68-85. https://doi.org/10.3390/ceramics7010006.
18. **Chen, Z.; Li, Z.; Li, J.; Liu, C.; Lao, C.; Fu, Y.; Liu, C.; Li, Y.; Wang, P.; He, Y.** 2019. 3D printing of ceramics: A review, Journal of the European Ceramic Society, 39(4), 661-687. https://doi.org/10.1016/j.jeurceramsoc.2018.11.013.
19. **Xie, Y.; Hill, C. A. S.; Xiao.; Militz, H.; Mai, C.** 2010. Silane coupling agents used for natural fiber/polymer composites: A review, Composites Part A: Applied Science and Manufacturing 41(7): 806-819. http://dx.doi.org/10.1016/j.compositesa.2010.03.005.
20. **Lacelle, T.; Sampson, K. L.; Sarvestani, H. Y.; Rahimizadeh, A.; Robles, J. B.; Mirkhalaf, M.; Rafiee, M. Jakubinek, M. B.; Paquet, C.; Ashrafi, B.** 2023. Additive manufacturing of polymer derived ceramics: Materials, methods, and applications, APL Materials 11(7): 070602. https://doi.org/10.1063/5.0151661.
21. **Hildebrand, G.; Sänger, J. C.; Schirmer, U.; Mantei, W.; Dupuis, Y.; Houbertz, R.; Liefeith, K.** 2021. Process Development for Additive Manufacturing of Alumina Toughened Zirconia for 3D Structures by Means of Two-Photon Absorption Technique, Ceramics 4(2), 224-239. https://doi.org/10.3390/ceramics4020017.
22. **Malagutti, L.; Ronconi, G.; Zanelli, M.; Mollica, F.; Mazzanti, V.** 2022. A Post-Processing Method for Improving the Mechanical Properties of Fused-Filament-Fabricated 3D-Printed Parts, Processes 10(11): 2399. https://doi.org/10.3390/pr10112399.
23. **Astakhov, V. P.; Xiao, X.** 2016. The Principle of Minimum Strain Energy to Fracture of the Work Material and Its Application in Modern Cutting Technologies, in Metal Cutting Technologies: Progress and Current Trends, ed. J. P. Davim. Berlin, Boston: De Gruyter Oldenbourg. 1–35p. https://doi.org/10.1515/9783110451740-004.
24. **Callister, W. D.; Rethwisch, D. G.** 2018. Fundamentals of Materials Science and Engineering, 5th Edition. John Wiley & Sons Inc. 960p.
25. **Nye, J. F.** Physical Properties of Crystals: Their Representation by Tensors and Matrices. 1985. New York: Oxford University Press. 352p.
26. **ASTM International,** ASTM E1876-19 Standard Test Methods for Dynamic Young's Modulus, Shear Modulus, and Damping in Metals (ASTM International, West Conshohocken, PA, 2019)
27. **Hibbeler, R. C.** 2016. Mechanics of Materials. Pearson Education. 896p.
28. Standard Test Method for Flexural Properties of Manufactured Carbon and Graphite Fiber Sheet Materials, ASTM D790 (ASTM International, West Conshohocken, PA, 2019).
29. **Boffoue, M. O.; Traore, B.; Kouakou, C. H.; Atcholi, K. E.; Lachat, R.; Ouratara, S.; Emeruwa, E.** 2017. Experimental Determination of the Poisson's Ratio and the Elastic Modulus of a Sand-Plastic Composite Material, International Journal of Engineering Research 6(6): 292-297.

http://dx.doi.org/10.5958/2319-6890.2017.00021.6.
30. **Plesha, M.; Gray, G.; Witt, R. J.; Costanzo, F.** 2022. Engineering Mechanics: Statics and Dynamics. McGraw-Hill Higher Education. 3557p.
31. **Yoshihara, H.; Yoshinobu, M.** 2015. Young's modulus and shear modulus of solid wood measured by the flexural vibration test of specimens with large height/length ratios, Holzforschung 69(4): 493-499. https://doi.org/10.1515/hf-2014-0151.
32. **Višniakov, N.; Škamat, J.; Černašėjus, O.; Kilikevičius, A.** 2020. Flash Welding of Microcomposite Wires for Pulsed Power Applications, Metals 10(8): 1053. https://doi.org/10.3390/met10081053.
33. **Rimša, V.; Kilikevičius, A.** 2021. Investigation of the effect of a flapping propeller on its aerodynamic performance, Mathematics 9(11): 1182. https://doi.org/10.3390/math9111182.
34. Phrozen Sonic Mini Resin 3D Printer technical data. Available at: https://phrozen3d.com/products/sonic-mini.

A. Shahidi, K. Stravinskas, A. Steponaviciute, A. Kilikevicius, D. Vainorius, J. Matijosius, O. Kapustynskyi, G. Mordas

ELASTICITY STUDY OF SLA ADDITIVELY MANUFACTURED COMPOSITES

S u m m a r y

The paper investigates the elasticity study of ceramic and photopolymer composites created using stereolithography (SLA) 3D printing, focusing on comparing "Liqcreate Composite-X" and "Phrozen's Water-Washable Resin." Dynamic flexural vibration tests were used to determine the natural frequencies and calculate the Young's moduli of the materials.

Keywords: ceramic composites, photopolymer composites, SLA 3D printing.

Received May 30, 2024
Accepted October 22, 2024